Science of the Total Environment 695 (2019) 133787

Contents lists available at ScienceDirect

Science of the Total Environment

journal homepage: www.elsevier.com/locate/scitotenv

Evaluation of a satellite-derived model parameterized by three soil moisture constraints to estimate terrestrial latent heat flux in the Heihe River basin of Northwest China

Yunjun Yao [a], Yuhu Zhang [b,*], Qiang Liu [c], Shaomin Liu [d], Kun Jia [a], Xiaotong Zhang [a], Ziwei Xu [d], Tongren Xu [d], Jiquan Chen [e], Joshua B. Fisher [f]

[a] State Key Laboratory of Remote Sensing Science, Faculty of Geographical Science, Beijing Normal University, Beijing 100875, China
[b] College of Resource Environment and Tourism, Capital Normal University, Beijing 100048, China
[c] College of Global Change and Earth System Science, Beijing Normal University, Beijing 100875, China
[d] State Key Laboratory of Earth Surface Processes and Resource Ecology, Faculty of Geographical Science, Beijing Normal University, Beijing 100875, China
[e] CGCEO/Geography, Michigan State University, East Lansing, MI 48823, USA
[f] Jet Propulsion Laboratory, California Institute of Technology, 4800 Oak Grove Dr., Pasadena, CA 91109, USA

HIGHLIGHTS

- A satellite-derived hybrid LE model was developed from *MODIS* and reanalysis data.
- Three *SM* constraints schemes exhibited some *LE* modeling differences.
- Different *SM* constraint schemes could impact the regional *LE* simulation.

GRAPHICAL ABSTRACT

Multiyear (2013–2015) mean seasonality of estimated *LE* across the Heihe River Basin.

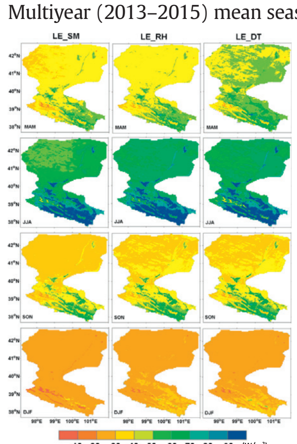

ARTICLE INFO

Article history:
Received 24 March 2019
Received in revised form 2 August 2019
Accepted 4 August 2019
Available online 06 August 2019

Editor: Ashantha Goonetilleke

Keywords:
Terrestrial latent heat flux
MODIS

ABSTRACT

Satellite-derived terrestrial latent heat flux (*LE*) models are useful tools to understand regional surface energy and water cycle processes for terrestrial ecosystems in the Heihe River basin (*HRB*) of Northwest China. This study developed a satellite-derived hybrid *LE* model parameterized by three soil moisture (*SM*) constraints: *SM*, relative humidity (*RH*), and diurnal air temperature range (*DT*); and assessed model performance and sensitivity. We used MODerate Resolution Imaging Spectroradiometer (*MODIS*) and eddy covariance (*EC*) data from 12 *EC* flux tower sites across the *HRB*. The hybrid model was trained using observed *LE* over 2012/2013–2014, and validated using observed *LE* for 2015 and leave-one-out cross-validation. The results show that the three *SM* constraints schemes exhibited some modeling differences at the flux tower site scale. *LE* estimation using *SM* achieved the highest correlation ($R^2 = 0.87$, $p < 0.01$) and lowest root mean square error ($RMSE = 20.1$ W/m^2) compared to schemes using *RH* or *DT* schemes. We then produced regional daily *LE*

* Corresponding author at: Capital Normal University, Beijing 100048, China.
E-mail address: yuhu.zhang@cnu.edu.cn (Y. Zhang).

https://doi.org/10.1016/j.scitotenv.2019.133787

Soil moisture constraints
Heihe River basin

maps at 1 km × 1 km across the *HRB* for 2013–2015. Regional analysis shows that our *LE* estimates from all three constraint models exhibited large spatial variability and strong seasonal and annual variations, attributed to differences in parameterizing the model water constraints. This study provides data and model based evidence to improve satellite-derived hybrid *LE* models with regard to water constraints.

1. Introduction

Terrestrial latent heat flux (*LE*) plays an important role in exchanges of water, energy and carbon cycles in the terrestrial ecosystem (Wang and Dickinson, 2012). Terrestrial *LE* has noticeably shifted for many regional *LE* estimation models, due to climatic change and human activities, which influences regional water cycles, vegetation growth, and climate change feedback, particularly in arid and semiarid regions (Fisher et al., 2017; Liu et al., 2018a; Zhou et al., 2018). Therefore, accurate regional *LE* quantification in arid and semiarid regions is crucial for water resource management, ecosystem conservation, and adaption strategies to climate change.

The Heihe River basin (*HRB*) is a typical oasis-desert arid region, particularly susceptible to surface energy and water cycle process changes due to increased agricultural irrigation, population expansion, and economic development (Liu et al., 2018a; Song et al., 2018; McVicar and Jupp, 2002; Mu et al., 2007; Wang and Dickinson, 2012; Yao et al., 2013; Priestley and Taylor, 1972). The Chinese scientific community has monitored terrestrial *LE* and eco-hydrological processes in the *HRB*, as part of the Heihe Plan launched by the National Natural Science Foundation of China (*NSFC*), including the watershed allied telemetry experimental research (*WATER*) and Heihe watershed allied telemetry experimental research (*HiWATER*) programs (Li et al., 2009a, 2009b; Li et al., 2013; Liu et al., 2018a; Cheng et al., 2014). Although these experiments provide accurate point measurements using eddy covariance (*EC*) methods, they may not represent large areas due to terrestrial ecosystem heterogeneity and dynamic heat transfer processes (Baldocchi et al., 2001; Twine et al., 2000; Wang et al., 2007).

Remote sensing has greatly improved regional scale soil and vegetation dynamics observations linked to terrestrial *LE* over heterogeneous ecosystems. Many satellite-derived *LE* products are available, including the MODerate-resolution Imaging Spectroradiometer (*MODIS*) *LE* (*MOD16*) (Mu et al., 2011; Yao et al., 2014; Jung et al., 2010; Zhang et al., 2010). Although *MOD16* has relatively high spatial (1 km) and temporal (8-day) resolution, validations have indicated that it retains significant uncertainties for most *EC* flux tower sites and *LE* values for the *HRB* are omitted (Hu et al., 2015a; Yao et al., 2017a; Mu et al., 2011; Xiong et al., 2015).

Various satellite-derived methods have been developed to estimate regional terrestrial *LE*, including empirical methods (Jackson et al., 1977; Jung et al., 2011; Nagler et al., 2005; Yang et al., 2006; Yao et al., 2015), physical models (e.g. surface energy balance (*SEB*) models, Penman-Monteith (*PM*) logic, Priestley-Taylor (*PT*) approach) (Norman et al., 1995; Anderson et al., 2008; Cleugh et al., 2007; Mu et al., 2011; Zhang et al., 2010; Fisher et al., 2008; Yao et al., 2017b; Miralles et al., 2011), data assimilation models (Pipunic et al., 2008; Xu et al., 2011a, 2011b), and distributed hydrology and land surface models based on satellite and meteorological data (Overgaard et al., 2006; Xie et al., 2015). Comprehensive reviews of the models development and validation accuracies are provided elsewhere (Kalma et al., 2008; Li et al., 2009a, 2009b; Wang and Dickinson, 2012; Ershadi et al., 2014; Polhamus et al., 2012; Badgley et al., 2015). However, not all models are equally good, providing a range of *LE* estimates at site and regional scales. For example, Wang and Dickinson (2012) reported that globally averaged *LE* estimates varied from 24.1 W/m^2 to 42.0 W/m^2 from 17 models. Similarly Ershadi et al. (2014) compared four models for various land cover types and showed that no single model was consistently best across all biomes. Model results were verified with low confidence at regional and site scales due to three main limitations: (1) surface landscape and terrestrial ecosystem process heterogeneity, (2) physiological parameter calibrations in the model, and (3) inadequate validation against ground measurements (Baldocchi et al., 1996; Yuan et al., 2010).

Satellite derived hybrid *LE* models may have the best potential to adequately simulate *LE* over a wide range of soil moisture (*SM*) content and land cover type, because they combine physical models and calibrated coefficients using ground observations from different ecosystems. For example, Wang et al. (2007) proposed a simple hybrid method to estimate terrestrial *LE* by relating ground-measured *LE* to net radiation (LE/R_n) from the *US* Atmospheric Radiation Measurement (*ARM*) to normalized difference vegetation index (*NDVI*) and air temperature (T_a). This method was consistent with the *PT* equation while incorporating vegetation influence on *LE*. However, the proposed method ignored *SM* impact on *LE* and overestimated *LE* during severe drought conditions. Subsequently Wang and Liang (2008) took into account the influence of *SM* on *LE* by incorporating diurnal T_a range (*DT*). Yao et al. (2015) used the combination of air relative humidity (*RH*) and atmospheric vapor pressure deficit (*VPD*) to parameterize *SM* effects on *LE* in a satellite-derived hybrid algorithm. Purdy et al. (2018) used *SM* from the Soil Moisture Active Passive Mission (*SMAP*) with the *PT-JPL* model (*PT* model provided by the Jet Propulsion Laboratory, *USA*), and demonstrated improved performance for semi-arid ecosystems. However, performance for satellite-derived hybrid *LE* models parameterized by different *SM* constraints remains unclear, particularly for the *HRB*, which incorporates large barren or sparsely vegetated areas. Thus, effects from employing surface *SM*, *RH*, and *DT* to characterize *SM* constraints for hybrid *LE* model performance require further evaluation for *HRB*.

In this study, we developed a satellite derived hybrid *LE* model parameterized by *SM*, *RH*, and *DT* soil moisture constraints in *HRB*, and assessed model performance. The objectives of this study are threefold: (1) to develop a satellite-derived hybrid *LE* model based on site-specific flux tower and *MODIS* data for *HRB*, and validate the model using eddy flux data in temporal and spatial domains; (2) to assess performance for the hybrid *LE* model parameterized by *SM*, *RH*, and *DT* constraints; and (3) to examine regional *LE* patterns using *SM*, *RH*, and *DT* constraints for 2013–2015.

2. Materials and methods

2.1. Research area

HRB is located on the northern slopes of the Qilian Mountains between 37.7°–42.7°N and 97.1°–102.0°E, covering a land area of approximately 143, 200 km^2 (Fig. 1). *HRB* is the second largest inland river basin in arid Northern China, with the Heihe River originating in the Qilian Mountains (Liu et al., 2018a, 2018b). The river stream flows through the Hexi Corridor of Gansu Province and arrives at two terminal lakes in the Western Inner Mongolia Plateau desert (Xiong et al., 2015). Study area elevation decreases from 2000 to 5000 m upstream, 1000–3000 m midstream, and 800–1700 m to downstream, covering several biomes. Major land cover types in the upstream region are glacier (snow/ice, *SIN*), alpine meadow (grassland, *GRA*) and Qinghai spruce (evergreen needleleaf forest, *ENF*); midstream includes maize (cropland, *CRO*), and piedmont desert (barren lands, *BAR*); and downstream includes mixed forests (*MIF*), terminal lake (water body, *WAT*),

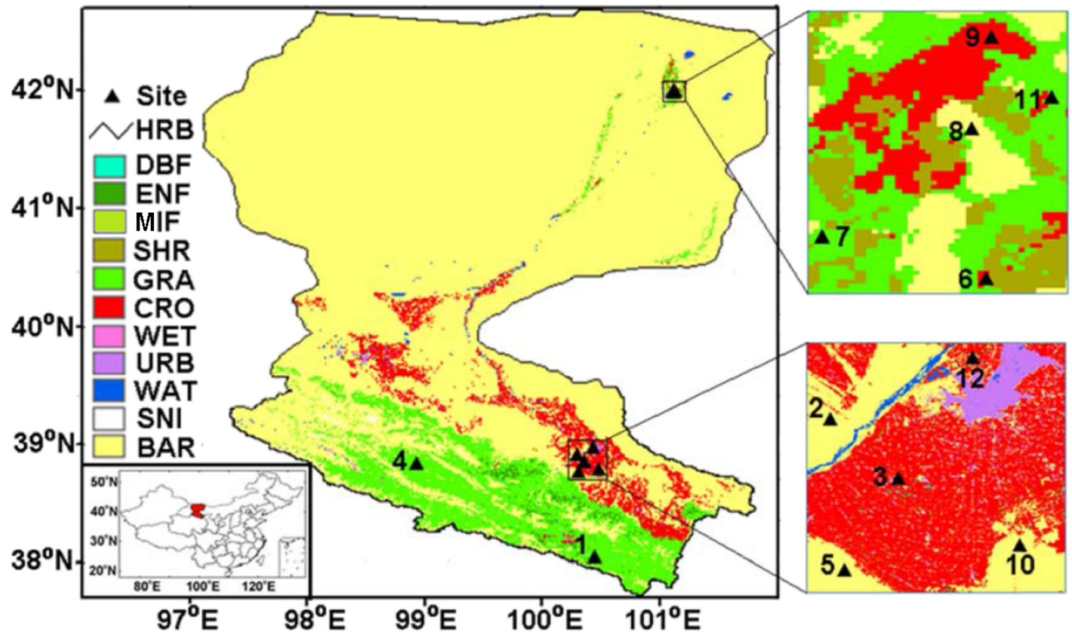

Fig. 1. Locations of 12 flux tower sites used in this study. The flux tower sites include 1. Arou; 2. Bajitan; 3. Daman; 4.Dashalong; 5. Huazhaizi; 6. Mixed forest; 7. Populus forest; 8. Barren-land; 9. Cropland; 10. Shenshawo; 11. Sidaoqiao; and 12. Zhangye. HRB refers to Heihe river basin boundary. The background image shows July 2015 land cover product from Landsat *TM* images. *DBF*: deciduous broadleaf forest; *ENF*: evergreen needleleaf forest; *MIF*: mixed forest; *SHR*: shrubland; *GRA*: grassland; *CRO*: cropland; *WET*: permanent wetland; *URB*: urban/build up; *WAT*: water body; *SNI*: snow/ice; and *BAR*: barren lands.

desert (*BAR*), and Populus euphratica and Tamarix (shrubland, *SHR*) (Li et al., 2018; Liu et al. 2018a). The region is dominated by continental arid climate with mean annual T_a increasing rapidly from 0.4 °C upstream to 7.3 °C midstream and 8.2 °C downstream. Annual precipitation (*P*) decreases gradually from 322.1 mm to 130.4 mm and 30.7 mm for the three reaches, respectively (Cheng et al., 2010; Song et al., 2018).

2.2. Data collection

2.2.1. Eddy covariance data

Eddy flux measurements for surface heat fluxes and corresponding meteorological data across *HRB* were used to assess model performance. Data from 12 *EC* flux tower sites in *HRB* provided by *WATER* and *HiWATER* experiments were collected to provide a data set covering 37 years (Liu et al., 2011; Liu et al., 2013; Xu et al., 2013). The *WATER* experiment incorporated a prototype hydrometeorology observatory network, with *EC* systems and automatic weather stations (*AWSs*) in upstream and midstream regions (Li et al., 2009a, 2009b). The subsequent *HiWATER* experiment established a comprehensive hydrometeorological observatory network across *HRB* upstream, midstream, and downstream regions in 2013 (Li et al., 2013; Liu et al. 2018a). Table S1 summarizes the 12 flux tower sites and Fig. 1 shows the site locations. Two flux tower sites were located upstream (Arou and Dashalong), five midstream (Bajitan, Daman, Huazhaizi, Shenshawo, and Zhangye), and five downstream (Mixed forest, Populus forest, Barren-land, Cropland and Sidaoqiao). Flux tower sites covered all six major land cover types: *GRA*, *CRO*, *BAR*, *MIF*, deciduous broadleaf forest (*DBF*), and permanent wetland (*WET*).

The data included half hourly surface net radiation (R_n), download solar radiation (R_s), soil heat flux (*G*), T_a, vapor pressure (*e*), maximum air temperature (T_{max}), minimum air temperature (T_{min}), relative humidity (*RH*), wind speed (*WS*), sensible heat flux (*H*), precipitation (*P*) and *LE*, which were subsequently aggregated into daily and monthly means. When missing data comprised <30% of the entire data for a given day, daily average was the numerical average of the measurements, otherwise daily average was treated as missing. Monthly data were similarly aggregated from the daily data. The data covered 2012–2015, with at least 2 years data from each flux tower. We used the Bowen ratio (*BR*) closure method to correct *LE* and *H* when processing *EC* data (Twine et al., 2000).

2.2.2. Remote sensing and reanalysis data

We used the *MODIS* 16-day *NDVI* product (*MOD*13*A*2) with 1-km spatial resolution (Huete et al., 2002) (http://daac.ornl.gov/MODIS/) and the 16-day albedo product with 1 km spatial resolution for 2013–2015 from the Global LAnd Surface Satellite (*GLASS*) product (http://glass-product.bnu.edu.cn) to develop a satellite derived hybrid *LE* model incorporating *SM*, *RH*, and *DT* for *LE* estimates across the entire watershed. Daily *NDVI* and albedo values were temporally linear interpolated from 16-day averages, and monthly land cover data with 30 m spatial resolution were used (Zhong et al., 2014).

We also used the global satellite-observed daily *SM* dataset (*ESA CCI SM*) to estimate regional *LE* in for *HRB*, part of the Climate Change Initiative (*CCI*) program with 0.25° spatial resolution from 2013 to 2015, a combined active and passive microwave product released by the European Space Agency (*ESA*) (Dorigo et al., 2017). Daily *ESA CCI SM* data were spatially interpolated to 1 km resolution using bilinear interpolation. Daily regional meteorological variables including T_a, T_{max}, T_{min}, R_s, and *RH* were simulated at 5 km spatial resolution using the weather research and forecasting (*WRF*) model combined with observations from China Meteorological Administration station (Pan et al., 2012). *WRF* is a next-generation, fully compressible, Euler non-hydrostatic mesoscale forecast model to derive meteorological parameters required for hydrological models. The model uses a terrain-following hydrostatic pressure coordinate system with permitted vertical grid stretching. Arakawa-C grid staggering is used for horizontal discretization. Skamarock and Klemp (2008) provide a detailed description for *WRF*. A one-way nested computational domain comprising 100 × 120 × 27 grid points with 5 km horizontal resolution was established previously by Pan et al. (2012). These weather data are freely accessible from the following website (http://westdc.westgis.ac.cn/data/). Regional meteorological variables were resampled from 5 × 5 km to 1 × 1 km resolution using bilinear interpolation.

Regional scale R_n was obtained following the method by Wang and Liang (2009). This model estimates the R_n from the surface albedo, daily R_s, T_{min}, DT, $NDVI$ and RH. Wang and Liang (2009) reported that the method used in their study to estimate R_n for 22 US sites yielded 19% relative error.

2.3. Remote sensing method

2.3.1. Satellite-derived hybrid LE model logic

We proposed a satellite-derived hybrid LE model based on the Wang and Liang (2008) model:

$$LE = R_n(k_0 + k_1 T_a + k_2 NDVI + k_3 f_s), \tag{1}$$

where k_i ($i = 0,\ldots,3$) is the empirical coefficient, which can be calibrated using ground-measurements and satellite data; and f_s is the SM constraint. In the Wang and Liang (2008) model, f_s refers exclusively to DT, whereas in the current study, f_s can refer to SM, RH, or DT because these variables reflect surface SM stress in different regions (Fisher et al., 2008; Wang and Liang, 2008; Wang et al., 2010; Yan and Shugart, 2010). Fig. S1 shows the hybrid LE model design, and empirical model coefficients were determined using surface meteorology and satellite data.

This satellite-derived hybrid LE model, characterized with LE/R_n, is a classical soil moisture and energy-limited LE regime (Seneviratne et al., 2010). In the energy-limited LE regime, corresponding to SM > threshold or critical value, LE/R_n is independent of SM content and f_s (SM, RH, or DT). This hybrid LE model varies less for SM saturated conditions and does not impact LE variability. In contrast, below the critical value, SM content provides a first-order constraint on LE/R_n in the soil moisture-limited LE regime. Incorporating f_s into the algorithm to estimate LE under insufficient-water conditions considers the effects of surface SM stress on terrestrial LE because f_s varies greatly for water-deficient surfaces, which strongly constrains LE/R_n variability and feedbacks to the atmosphere.

A satellite-derived hybrid LE model offers several advantages over complicated physical LE models, including providing easy routine and long term LE mapping because it only requires R_n, T_a, NDVI, and f_s, avoiding computational complexities of aerodynamic and surface resistance (Gao and Dirmeyer, 2006; McVicar et al., 2012; Yao et al., 2015); and reducing errors from forcing data by avoiding the use of the land surface temperature and T_a differences (Wang and Dickinson, 2012).

2.3.2. Model calibration and validation

We calibrated empirical coefficients for Eq. (1) using site specific MODIS and EC ground measured data. We split site level EC and MODIS datasets from the 12 flux tower sites into training (2012/2013–2014) and test (2015) datasets using the holdout method, providing 5113 and 2605 sample datasets, respectively. We evaluated model performance using root mean squared error (RMSE):

$$RMSE = \sqrt{\frac{1}{N}\sum_{i=1}^{N}(x_{is} - x_{io})^2}, \tag{2}$$

where x_{is} is the daily simulated LE, x_{io} is the daily observed LE, N is the number of samples. We then estimated RMSE and seasonal variations between estimated and observed LE.

We also assessed the proposed model performance in the spatial domain using leave one out cross-validation (Xiao et al., 2010), i.e., data from a single site was used for validation, after data from the remaining sites provided Eq. (1) calibration coefficients. Because calibration and validation data were from different sites that were generally several kilometers from each other, and spatial autocorrelation between sites was negligible, calibration and validation data were considered to be independent. The leave one out cross-validation was separately conducted for each site.

2.3.3. Regional LE estimation

As discussed above, since land cover types for the 12 EC flux tower sites included alpine meadow, cropland, Gobi, desert, wetlands, forests, and mixed cover (including vegetation and bare soil); and the locations differed from each other, ground-measured datasets were reasonable representative of typical HRB ecosystems and climate types. Thus, the proposed model developed from the 12 sites could be extrapolated to regional LE estimation across the whole HRB. We used the proposed model to estimate daily terrestrial LE for each 1 × 1 km cell across HRB for 2013–2015 using MODIS, ESA CCI SM, and WRF gridded meteorological data. Monthly estimated LE was calculated by averaging daily estimated LE. We examined regional LE patterns for 2013–2015 to compare model performance.

3. Results

3.1. Sensitivity of environmental regulators to LE

Data collected from 2012/2013–2014 were analyzed at 12 flux tower sites to identify environmental regulators from terrestrial LE variation. Table S2 summarizes the correlation coefficients between LE and surface R_n, T_a, RH, DT, SM, NDVI and P at the 12 sites. For all flux tower sites, R_n exhibited the highest correlation coefficient (r) with LE ($0.50 \le r \le 0.91$), with correlation coefficients between LE and T_a second highest ($0.46 \le r \le 0.84$), indicating R_n and T_a were the most essential controlling parameters to estimate terrestrial LE. NDVI and SM were also highly correlated to LE with correlation coefficients between LE and NDVI (and SM) for most flux tower sites >0.5(and 0.4). Therefore, NDVI and SM are also important parameters for determining terrestrial LE. In contrast, correlation coefficients between RH (and DT) and LE were relatively low because seasonal variation differ between RH (and DT) and LE. Cumulative P over 15 days was also highly correlated with LE for most flux tower sites ($0.35 \le r \le 0.65$) due to time lags between LE change and P occurrence for consecutive time periods.

Normalized terrestrial LE (LE/R_n) can also be used to develop LE models due to their near-linear relationship (Wang et al., 2007; Wang and Liang, 2008). Table 1 shows LE/R_n correlation coefficients with related parameters. For most flux tower sites, ground measured LE/R_n showed highest correlations with NDVI ($0.14 \le r \le 0.81$) and SM ($0.05 \le r \le 0.83$), with T_a ($0.12 \le r \le 0.80$), cumulated P over 15 days ($0.15 \le r \le 0.53$), RH ($0.02 \le r \le 0.67$), and DT ($-0.45 \le r \le -0.01$) subsequently. Although SM was weakly positive correlated to LE/R_n at three sites (Mixed forest, Populus forest and Barren-land), the high correlations between SM and LE/R_n at most sites indicated that SM influence on LE was larger than for near-surface meteorological conditions (RH and DT) in the HRB. Overall, after NDVI, SM had high potential capacity for

Table 1
Correlation coefficients between daily normalized LE (LE/R_n) and the daily SM ($r_{LR,\ SM}$), RH ($r_{LR,\ RH}$), NDVI($r_{LR,\ NDVI}$), T_a($r_{LR,\ Ta}$), DT ($r_{LR,\ DT}$) and cumulated P over 15 days. LR refers to normalized LE (LE/R_n).

Name	$r_{LR,\ SM}$	$r_{LR,\ RH}$	$r_{LR,\ NDVI}$	$r_{LR,\ Ta}$	$r_{LR,\ DT}$	$r_{LR,\ P}$
Arou	0.62	0.66	0.81	0.78	−0.45	0.46
Bajitan	0.50	0.40	0.43	0.23	−0.10	0.51
Daman	0.74	0.22	0.73	0.71	−0.04	0.53
Dashalong	0.83	0.61	0.82	0.80	−0.35	0.50
Huazhaizi	0.36	0.53	0.14	0.12	−0.20	0.40
Mixed forest	0.05	0.03	0.71	0.70	−0.04	0.04
Populus forest	0.27	0.02	0.58	0.79	−0.02	0.17
Barren-land	0.32	0.10	0.55	0.70	−0.01	0.20
Cropland	0.62	0.10	0.61	0.60	−0.02	0.15
Shenshawo	0.43	0.67	0.48	0.28	−0.27	0.29
Sidaoqiao	0.53	0.11	0.51	0.50	−0.14	0.49
Zhangye	0.73	0.10	0.75	0.71	−0.10	0.44
All	0.58	0.26	0.66	0.51	−0.02	0.39

determining LE/R_n variations across various land cover and environmental status types. *SM* was positively correlated with LE/R_n everywhere, and had the largest overall correlation for almost all flux tower sites, whereas *DT* was negatively correlated with LE/R_n everywhere, and had the lowest overall correlation (Table 1).

However, the correlations differed greatly between tower sites. For example, LE/R_n showed strong correlation with *RH* at two desert sites (Huazhazi and Shenshawo), suggesting that *RH* may capture the water stress for *LE* estimation on bare land (desert), whereas *RH* and LE/R_n were only weakly correlated at the two forests sites (Mixed forest and Populus forest), suggesting that *RH* may not successfully characterize *LE* at forest sites.

3.2. Model evaluation using three soil moisture constraints

3.2.1. Model evaluation based on the holdout method

Fig. 2 shows performance for the hybrid *LE* model parameterized by *SM*, *RH*, and *DT* using the training dataset (2012/2013–2014) collected at the 12 flux tower sites, covering a wide range of land cover types. The *SM* constrained schemes exhibited *LE* model differences at the flux tower site scale. *LE* estimation using *SM* (*LE_SM*) achieved the highest $R^2 = 0.87$ ($p < 0.01$) and lowest $RMSE = 20.1$ W/m^2 compared with *LE* estimation using *RH* (*LE_RH*) and *DT* (*LE_DT*); with *LE_DT* achieving the lowest $R^2 = 0.81$ ($p < 0.01$) and largest $RMSE = 22.1$ W/m^2. Hybrid *LE* models using different *SM* constraint schemes

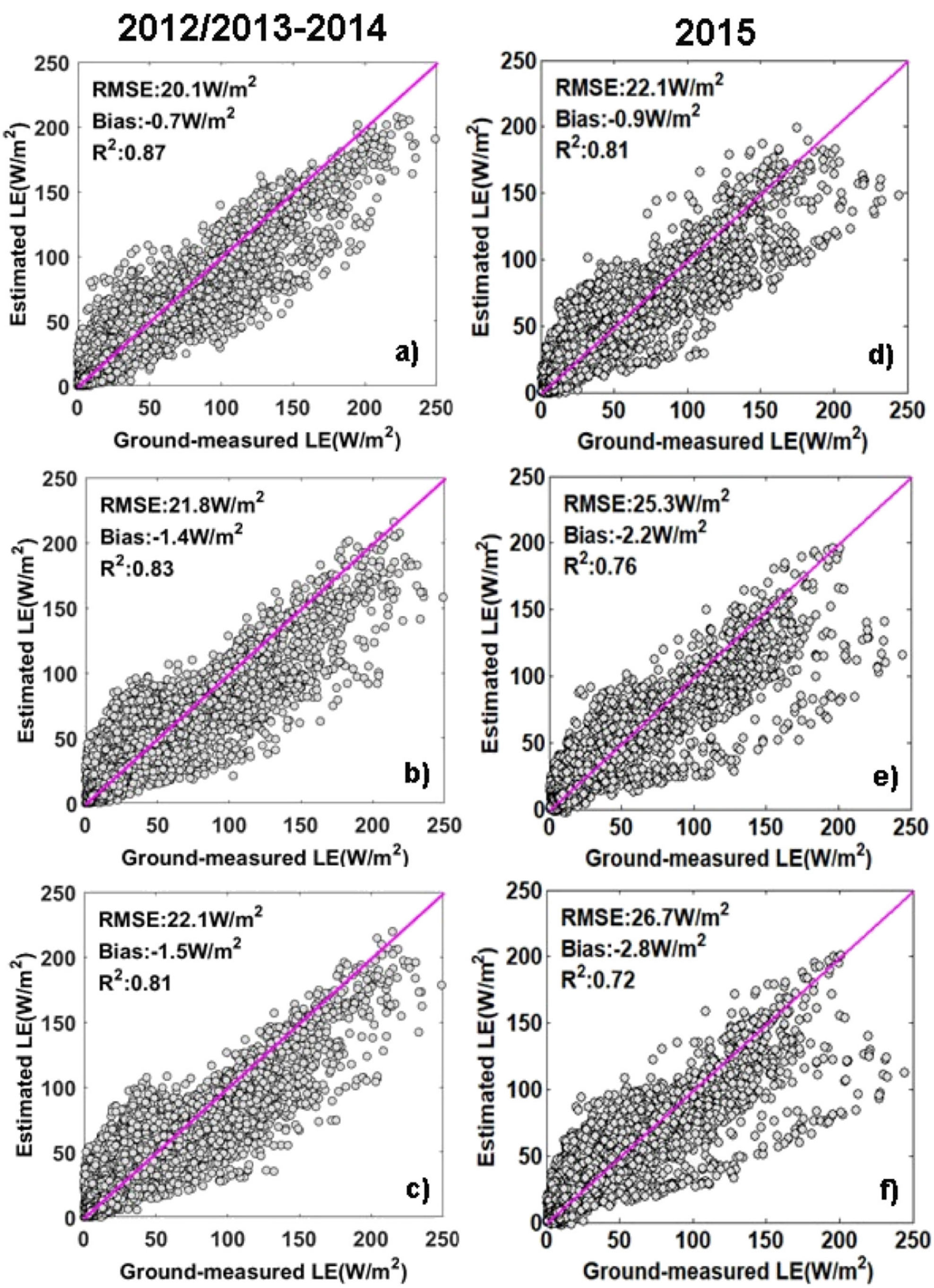

Fig. 2. Scatterplots of observed daily *LE* versus estimated daily *LE* for 2015. The estimated *LE* was calculated using the coefficients for Eq. (1) for 2012/2013–2014. a) *LE_SM*; b) *LE_RH* and c) *LE_DT*.

performances for the test dataset (2015) were similar to the training dataset (Fig. 2), although *RMSE* and R^2 were slightly poorer [22.1 W/m^2 and 0.81 ($p < 0.01$), 25.3 W/m^2 and 0.76 ($p < 0.01$), and 26.7 W/m^2 and 0.72 ($p < 0.01$) for *LE_SM*, *LE_RH*, and *LE_DT*, respectively]. Validation tests showed that *LE_SM* decreased *RMSE* by >3.2 W/m^2, and increased R^2 by >0.05 ($p < 0.01$) compared with *LE_RH* and *LE_DT*.

Fig. 3 compares *LE* estimates using the *SM* constraint schemes with observed *LE* for each flux tower site for 2015. The estimates captured most *LE* seasonal features through 2015, aside from exceptionally high *LE* for some sites, e.g., Mixed forest and Populus forest sites. Model performance between the *SM* constraint schemes also varied with site. The schemes all exhibited large overestimation for Barren land and large underestimation for the Sidaoqiao site; with other forest and cropland sites only showing moderate underestimation over June to August. In contrast, the Shenshawo site underestimation occurred for winter 2015 and Barren land overestimation occurred in other periods. *LE_SM* produced the closest seasonal *LE* variations to ground observed values compared with *LE_RH* and *LE_DT* for most flux tower sites.

Fig. 4 shows the superior capacity of the proposed model to predict *LE* spatial variation by comparing estimated and measured site average daily *LE* for 2015 at the 12 flux tower sites. The proposed models estimated *LE* reasonably (R^2 = 0.75, 0.62, and 0.55; and *RMSE* = 14.3, 18.4, and 19.3 W/m^2, respectively) although they all greatly underestimated *LE* at Sidaoqiao. *LE_SM* achieved the highest accuracy according to *LE* spatial variation validation. Therefore, regional *LE*

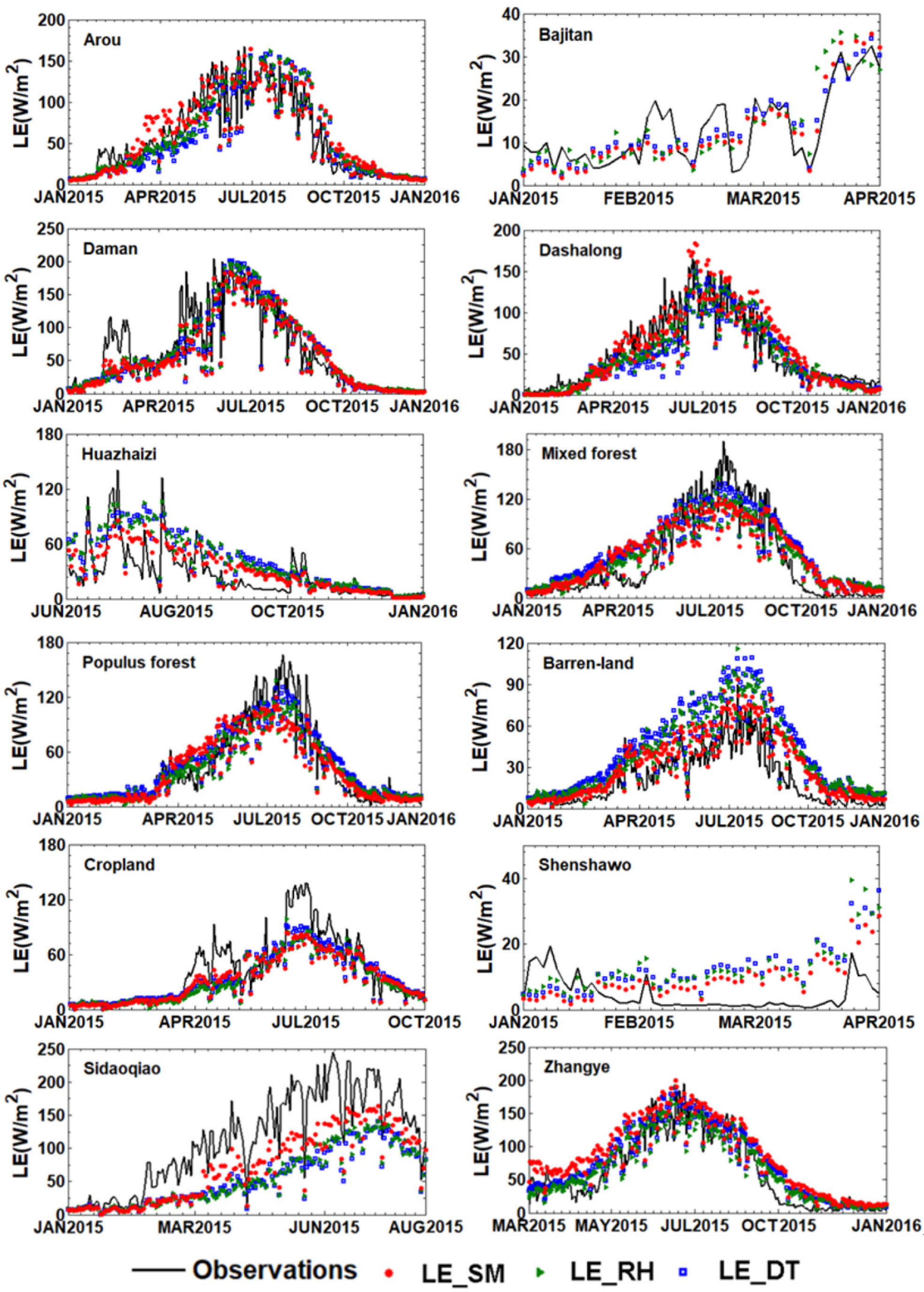

Fig. 3. Daily variation of estimated and ground measured latent heat of evaporation (*LE*) variation from *EC* measurements for 2015. The estimated *LE* was calculated using the coefficients for Eq. (1) for 2012/2013–2014.

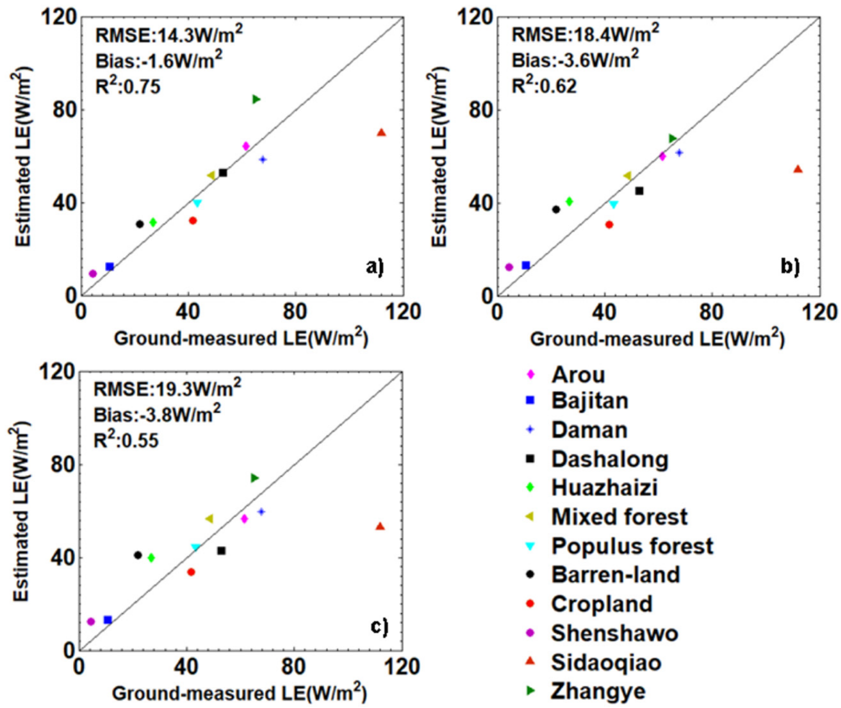

Fig. 4. Comparisons of estimated and measured site averaged daily *LE* for 2015 at 12 flux tower sites: (a) *LE_SM*, (b) *LE_RH*, and (c) *LE_DT*.

simulation may be acceptable by adjusting Eq. (1) coefficients to local conditions with relatively sparse ground observations.

3.2.2. Model evaluation using leave-one-out cross-validation

We then validated the models in the spatial domain using leave one out-cross- validation. Fig. 5 shows that all proposed models (*LE_SM*, *LE_RH*, and *LE_DT*) estimated *LE* fairly well, though model performance varied with site and biome type. Generally, higher performance was achieved for *GRA* (meadow) and *CRO* (maize) ecosystems than *MIF*, *DBF* (Populus forest), and *SHR* (*Tamarix chinensis*). Overall, *LE_SM* exhibited slightly better performance compared to ground measurements than *LE_RH* and *LE_DT* at most flux tower sites, achieving approximately 7.8% higher R^2 ($p < 0.01$), and 8.2% smaller *RMSE*.

Fig. S3 shows the proposed model had a good ability to estimate *LE* spatial variation. Site averaged *LE_SM* estimates for different biome *LEs* at the 12 sites achieved superior $RMSE = 6.8$ W/m^2 and $R^2 = 0.89$ ($p < 0.01$), compared with *LE_RH* ($RMSE = 10.5$ W/m^2, $R^2 = 0.77$, $p < 0.01$) and *LE_DT* ($RMSE = 10.9$ W/m^2, $R^2 = 0.73$, $p < 0.01$). *SM* constraints in the hybrid *LE* model generally improved model performance compared with *RH* and *DT* constraints for most flux tower sites and land cover types.

Temporal and spatial domain validation verified that the performance of our proposed model using three *SM* constraints schemes was particularly encouraging, across ecosystem types, structures, and management practices. The model used *EC* flux tower data, and included typical *HRB* ecosystems and climate types. Thus, the proposed hybrid model has potential to upscale flux tower *LE* data to regional scale across *HRB*.

3.3. Regional LE estimation using three soil moisture constraints

3.3.1. Regional implementation of the LE model

We implemented the satellite-derived hybrid *LE* model in the *HRB* to further demonstrate its robustness. We recalibrated Eq. (1) coefficients using the *MODIS* products, ground measured meteorological variables, and *LE* data collected at all 12 flux tower sites. Table 2 lists Eq. (1) parameters for all biomes by linear regression based on *MODIS* derived *NDVI*, ground measured T_a, and *RH*, and *DT*, and *SM*. Because of the different land cover types and locations of the 12 *EC* flux tower sites, we found the models sufficiently representative to estimate regional *LE* across the *HRB*.

Fig. 6 compares daily estimated *LE* derived from tower specific meteorology and ground measured *LE* at all 12 flux tower sites, with *RMSE* = 21.1, 23.1, and 24.2 W/m^2; and $R^2 = 0.85$, 0.80, and 0.78 (all $p < 0.01$) for *LE_SM*, *LE_RH* and *LE_DT*, respectively. Monthly estimated *LE* showed good correlation to ground measured *LE* at all 12 flux tower sites, with $RMSE = 15.8$ W/m^2, 18.5 W/m^2, and 19.9 W/m^2; and $R^2 = 0.89$, 0.84, and 0.81 at the 99% level of confidence, respectively. Similar outcomes were found for estimated daily and monthly *LE* derived from *WRF* reanalysis, *MODIS*, and *ESA CCI SM* data (Fig. S3). Thus, estimated *LE* from the proposed approach could be applied to estimate regional terrestrial *LE* across *HRB* for 2013–2015.

3.3.2. Seasonal and annual LE patterns

Daily *LE* estimates from the proposed approach were highly constrained by eddy flux data, and provided spatially and temporally continuous *LE* across *HRB*, allowing seasonal and annual *LE* patterns to be investigated. Fig. 7 shows multiyear (2013–2015) mean seasonality for *LE_SM*, *LE_RH* and *LE_DT* model estimates. *LE* exhibited large spatial variability and strong seasonal fluctuations reflecting controlling effects from climate conditions. In the spring months (March–May), *LE* in the upstream and midstream area was higher than downstream as temperature gradually increased and vegetation growth commenced. In the summer months (June–August), *LE* peaked due to favorable temperature and *SM* conditions, with summer precipitation accounting for approximately 80% of annual precipitation. In the fall months (September–November), *LE* substantially decreased relative to summer as temperature dropped and vegetation began to senesce. Spatial patterns and *LE* magnitude were similar to spring. In the winter months (December–February), *LE* values were lowest since the low temperature caused little or no photosynthesis as the vegetation was dormant.

Fig. S4 shows seasonal terrestrial *LE* spatial differences across the *HRB* (ΔLE_{SR} = *LE_SM-LE_RH*; ΔLE_{SD} = *LE_SM-LE_DT*; and ΔLE_{RD} = *LE_RH-LE_DT*). Relative to *LE_RH* and *LE_DT*, *LE_SM* yielded lower seasonal terrestrial *LE* across almost all *HRB* regions; whereas *LE_RH*

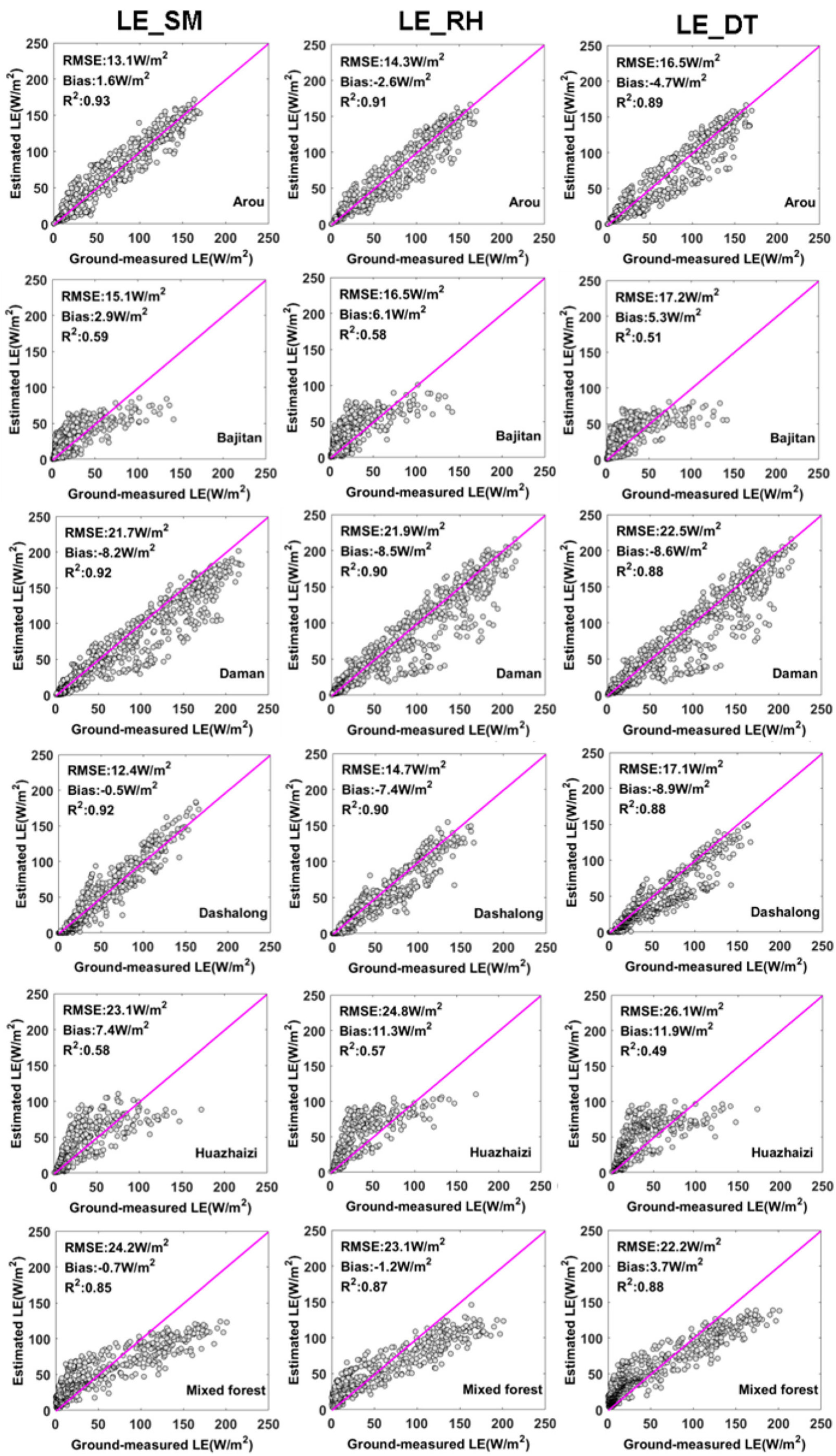

Fig. 5. Leave one out cross-validation for estimated daily LE models.

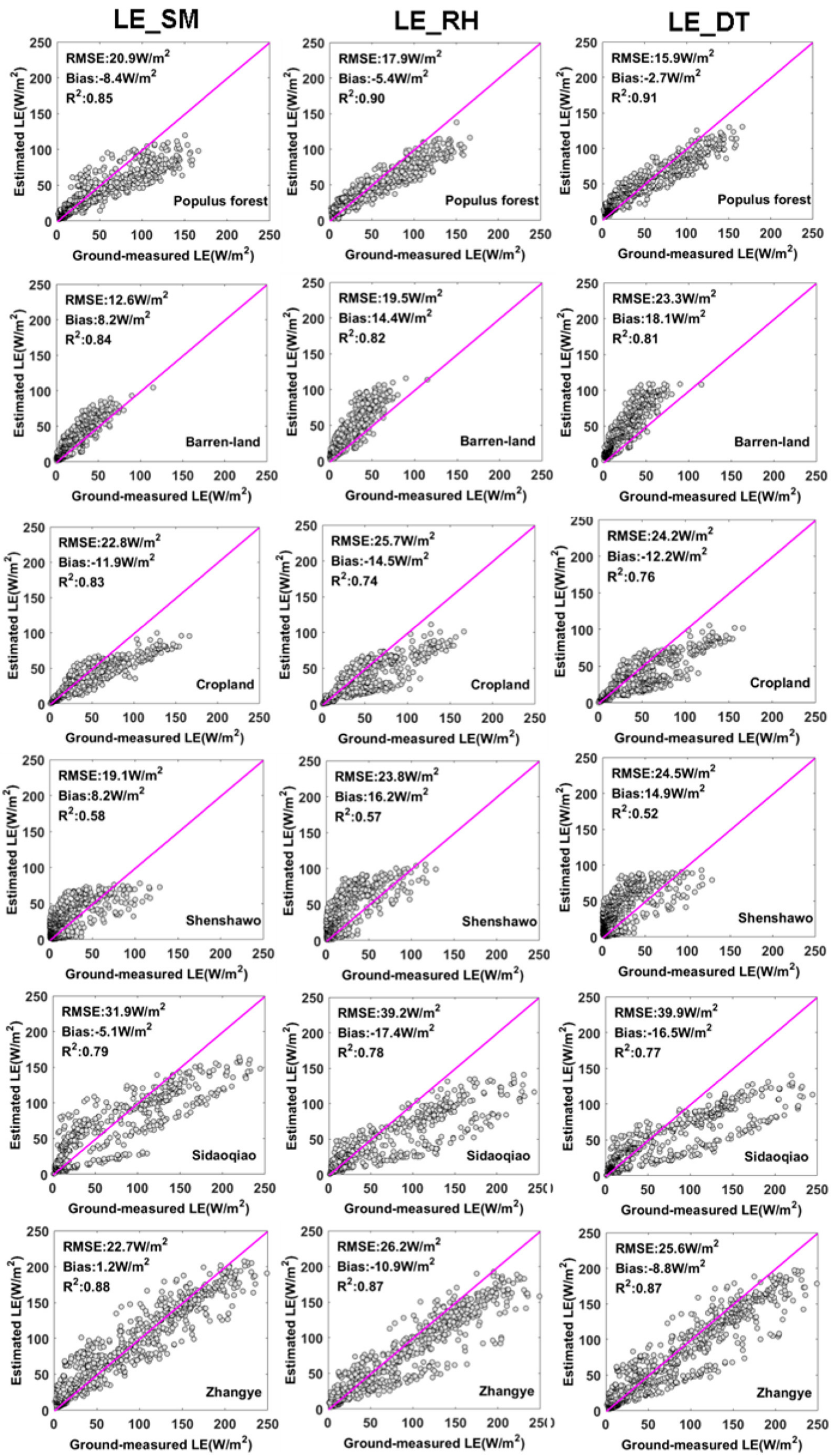

Fig. 5 (*continued*).

Table 2
Fitted parameters for Eq. (1) and related statistics for the tower sites. Eq. (1) was used to estimate daily *LE* at the sites using the parameters shown.

Combinations of parameters	*NDVI*, T_a, *SM*	*NDVI*, T_a, *RH*	*NDVI*, T_a, *DT*
K_0	0.036	−0.028	0.089
K_1	0.006	0.009	0.007
K_2	0.710	0.760	0.983
K_3	0.708	0.337	−0.001

exhibited higher seasonal terrestrial *LE* than *LE_DT* across almost all *HRB* regions from summer to winter, but lower than *LE_DT* during spring.

Fig. S5 shows calculated annual *LE_SM*, *LE_RH*, and *LE_DT* for 2013–2015 from daily *LE* estimates, and subsequent average annual *LE* over the period. Total *LE* for *LE_SM*, *LE_RH*, and *LE_DT* is 25.1 W/m^2, 29.6 W/m^2, and 30.3 W/m^2 for *HRB* over 2013–2015, respectively. Annual *LE* showed considerable spatial variation with large spatial gradient from south (upstream) to north (downstream), i.e., *LE* decreased along a gradient starting in the southern mountains, where vegetation coverage was abundant, through to sparse vegetation across the northern region, which is largely semiarid climate (Xiong et al., 2015). Therefore, *LE* variation was consistent with regional climate and vegetation distributions.

Fig. S6 compares estimated annual *LE* from the proposed models for 2013–2015 across *HRB*. *LE_SM* exhibited lower annual terrestrial *LE* for almost all regions compared with *LE_RH* and *LE_DT*; whereas *LE_RH* had higher annual *LE* than *LE_DT* for most upstream and downstream regions but lower *LE* across most midstream regions. The *LE_DT* model exhibited particularly low performance for water limited regions (desert regions).

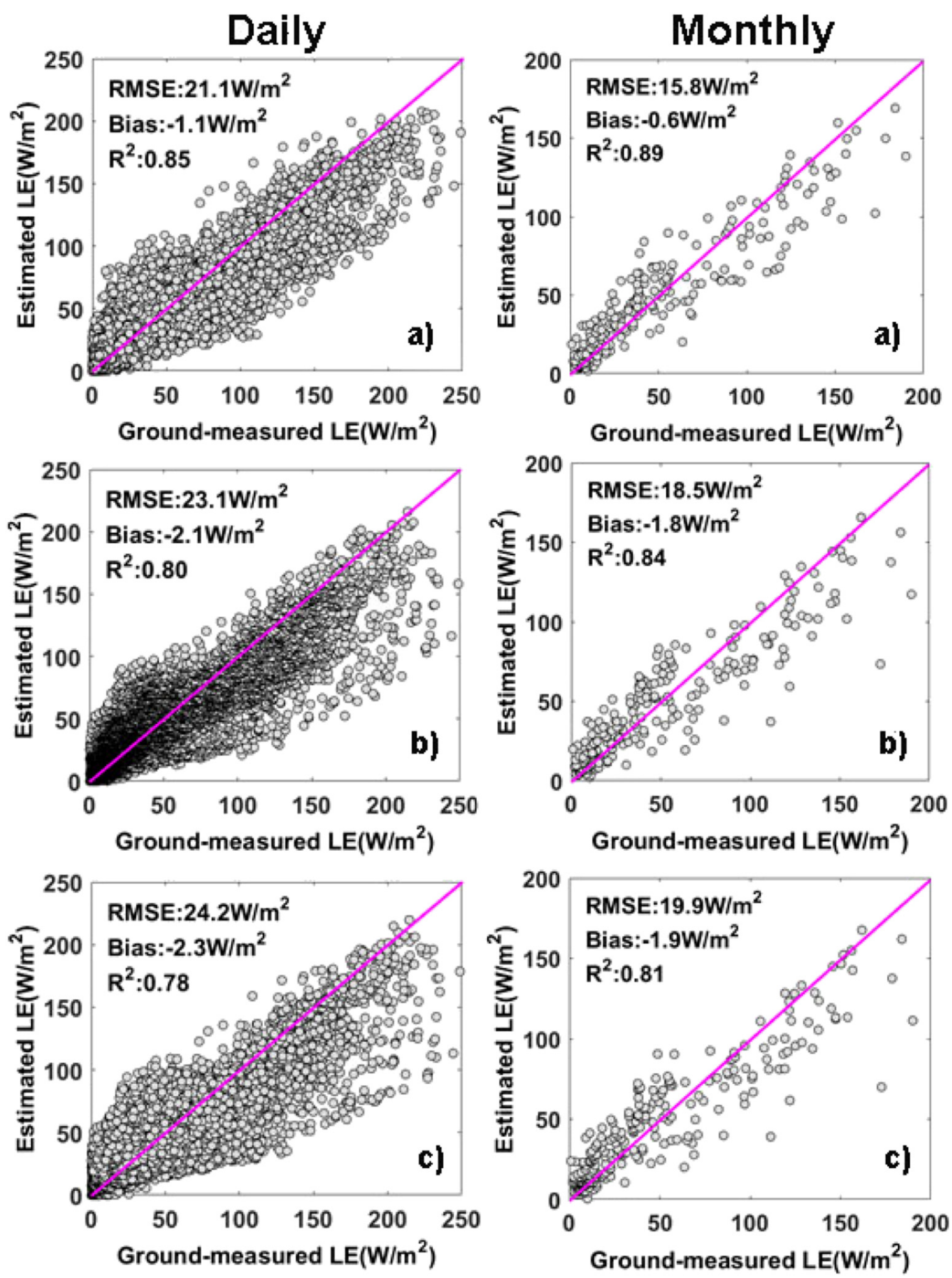

Fig. 6. Comparison of the estimated using tower-specific meteorology and measured daily and monthly *LE* collected at all 12 flux tower sites: (a) *LE_SM*, (b) *LE_RH*, and (c) *LE_DT*.

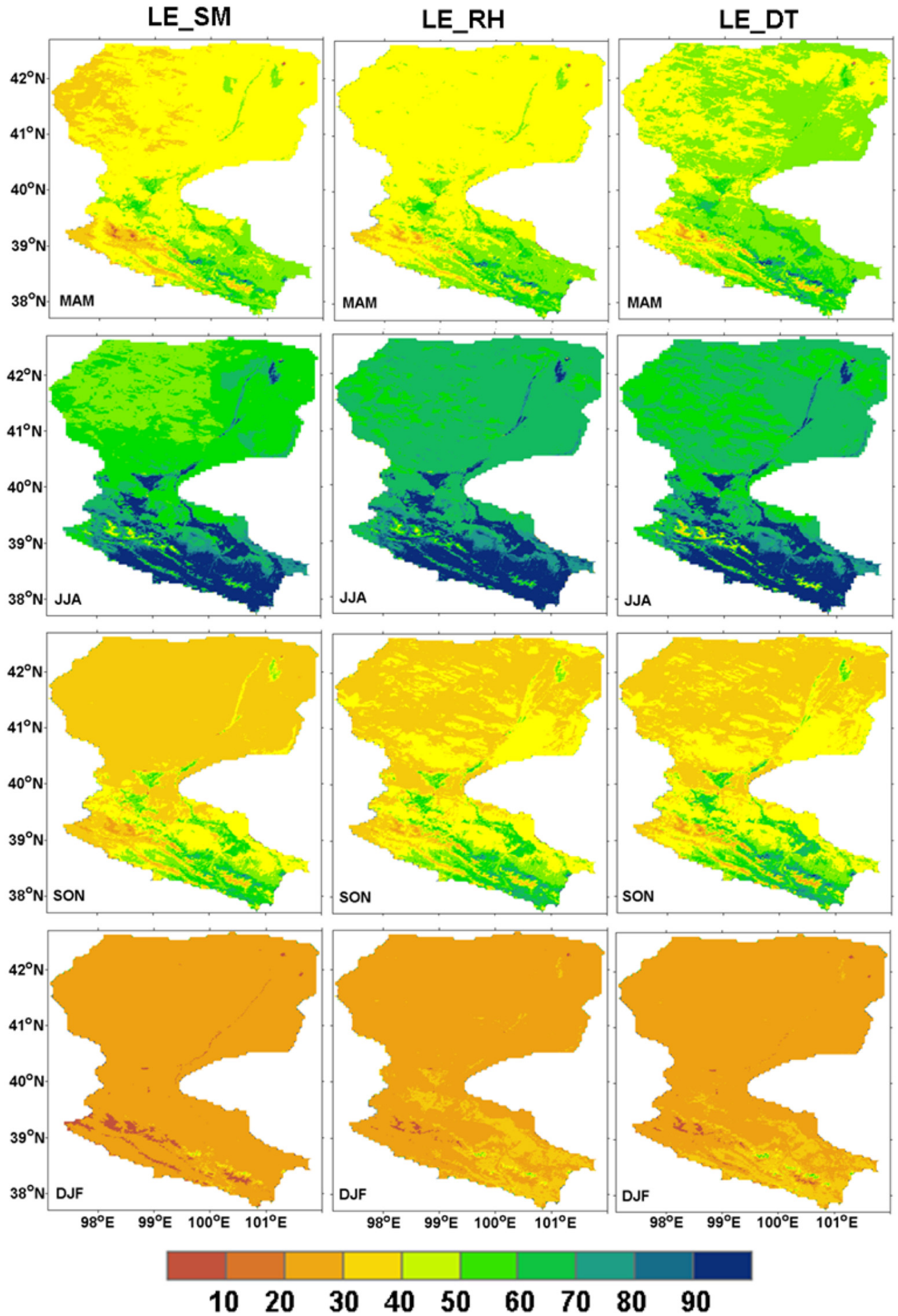

Fig. 7. Multiyear (2013–2015) mean seasonality of estimated *LE* across the Heihe River Basin. Units are in W/m^2.

4. Discussion

4.1. Model performance for different biomes

Previous studies have shown that satellite-derived hybrid *LE* models can achieve comparable accuracy to more complicated models (Jiménez et al., 2011; Kalma et al., 2008; Mueller et al., 2011; Wang and Dickinson, 2012; Yao et al., 2018) and, the model simplicity also allows regional application. However, the proposed hybrid *LE* models parameterized by *SM*, *RH*, and *DT* differed over various biomes and conditions. For example, all the proposed hybrid *LE* models achieved high performance at Arou, Daman, Dashalong, and Zhangye sites, which may be partially attributed to the model successfully capturing seasonal *LE* variation reflected by the strong *NDVI* seasonality for grass (meadow) and crops (Yebra et al., 2013). Vinukollu et al. (2011) and Ershadi et al. (2014) showed superior *PT* model performance, similar to satellite-derived hybrid *LE* models, for 12 *EC* towers located in grasslands and croplands over a three-year period using monthly averages of hourly data. However, significant bias was identified for the growing season (summer). In contrast, the proposed hybrid *LE* models achieved relatively low performance for most forest sites because rising groundwater levels due to the ecological water diversion project (*EWDP*) induced *LE* changes and the models did not consider groundwater effects on *LE* (Zhou et al., 2018). Vegetation transpiration can extracts groundwater from the rooting zone down to tens of meters or more when available soil water is low (Wang and Dickinson, 2012). For example, *LE* for the forested area (in the middle of the study region), which had high groundwater level, was higher than that in lower areas where vegetation degradation was associated with artificial canals (Hu et al., 2015b).

Generally, *LE_SM* models achieved superior statistical agreement to observation compared with *LE_RH* and *LE_DT* models, which had relatively close agreement. However, *LE_SM* achieved lower accuracy compared with both *LE_RH* and *LE_DT* for Mixed forest and Populus forest sites, because *SM* was not the main *LE* controlling factor. Previous studies have shown that *RH* was more closely related to evaporation fraction (*EF*) than *SM* for several biomes (Yan and Shugart, 2010). García et al. (2013) also found that *SM* was the most sensitive constraint for energy driven *LE* models, contributing 22% to estimated *LE* uncertainty.

Satellite derived hybrid *LE* model bias was likely due to the following reasons. First, *EC* measurements have approximately 5–20% error (Foken, 2008; Glenn et al., 2008) and gap filling from half hourly data to daily means also adds approximately 5% error (Hui et al., 2004). *EC* measurements also have energy imbalances and we corrected *LE* using the Twine et al. (2000) method in this study; but, errors due to these effects remain unclear (Shuttleworth, 2007). Second, *MODIS NDVI* and tower footprints were not matched, hence vegetation signals at flux towers could significantly differ from those within the *MODIS* footprint (Xiao et al., 2010). Third, cloud cover caused significant missing daily *NDVI*, hence 16 day *NDVI* may not always represent valid average environmental conditions and fluxes over the period, causing *LE* underestimation or overestimation (Xiao et al., 2008). Finally, independent variables included in the model did not consider potentially significant other factors, e.g. wind speed or CO_2 levels, which could potentially reduce *LE* estimation errors by 5–10% (Idso and Brazel, 1984; McVicar et al., 2012).

4.2. Regulators impacts on model performance

Available energy, air temperature, and moisture demand were been considered as the three most important regulators controlling *LE*. The satellite-derived hybrid *LE* models correlated strongly with R_n because it represents the energy available to drive surface evaporation and vegetation transpiration, which varies with spatiotemporal *LE* variation in terrestrial ecosystems (Wang and Dickinson, 2012). However, R_n exerts greater influence on energy limited water yielding than water limited catchments (McVicar et al., 2012). Air temperature (T_a) is another key factor in determining *LE* for most ecosystems, particularly in alpine regions. Previous studies have shown that transpiration shows significant linear correlation with T_a in desert riparian forest and other extreme arid regions (Si et al., 2007). The present study confirmed high correlation between *LE* and T_a in *HRB*. Additionally, we used *NDVI* to develop the hybrid models because it can characterize spatial vegetation moisture variability. *LE* is significantly modulated by available water and vegetation canopy characteristics characterized by *NDVI* for unsaturated soil and vegetation surfaces with limited water supply (Fisher et al., 2008; Wang and Liang, 2008; Wang et al., 2010). Therefore, the hybrid *LE* models improved *LE* simulation accuracy by integrating satellite-derived vegetation parameters (*NDVI*).

Three variables (*SM*, *RH*, and *DT*) were used to parameterize *SM* constraints for the hybrid *LE* models. For hybrid model parameterized by *SM*, *SM* is directly used to optimize *SM* constraints. The *SM* in this study from ground observation covered 0–5 cm and *ESA CCI SM* generally covers layer depth as 0.5–2 cm, but *SM* from deeper soil layers contributed to water energy processes, which may be another reason for underestimation of the Mixed forest and *DBF* (Populus forest). Previous studies have shown explicit *SM* functions from different soil layers to be useful in parameterizing *LE* moisture controls (Jin et al., 2011; Brutsaert, 2005; Chen and Dudhia, 2001; Miralles et al., 2011). However, they cannot be applied when *SM* from different soil layers is unavailable. The proposed hybrid *LE* models parameterized by different *SM* constraints were complementary to other complicated approaches.

The proposed hybrid model used *RH* to characterize *SM* constraint based on the complementary Bouchet (1963) hypothesis, where surface moisture status was linked to and reflected atmospheric evaporative demands (Fisher et al., 2008; Yao et al., 2015; Yan and Shugart, 2010). Similarly, the hybrid models parameterized by *DT* used simplified apparent thermal inertia (*ATI*) characterized by temperature change, because *ATI* reflects surface *SM* variation (Zhang et al., 2003). However, *RH* and *DT* used in the hybrid models include uncertainties for optimizing *SM* constraints. First, they only account for effects due to air moisture concentration and atmospheric evaporation demand, ignoring surface *SM* supply impacts. Second, they are not good indicators for *SM* spatial heterogeneity across the landscape (Yao et al., 2017a). Therefore, *SM* constraint noise (*SM*, *RH*, or *DT*) will reduce hybrid *LE* model performance due to the complicated relationship between *SM* and soil evaporation. Future research will consider other biophysical variable effects on *SM* constraints for different biomes.

4.3. Regional LE estimation differences using different soil moisture constraints

Spatial differences among *LE_SM*, *LE_RH*, and *LE_DT* were much greater than those for regional mean values. The large discrepancies may be attributed to differences in water constraint parameterization for the model. Fig. S7 shows an example spatial distribution for interpolated monthly *SM* derived from the *ESA CCI* dataset, with *RH* and *DT* derived from reanalysis data for June 2013–2015 at 1 km spatial resolution. *SM*, *RH*, and *DT* had similar spatial distribution patterns reflecting surface moisture variations, although spatial distributions in Northwestern *HRB* exhibited small differences. Different *SM* constraint parameterizations could impact the simulation by partitioning surface energy flux differently (Robock et al., 2003; Wang and Liang, 2008).

Aside from *SM* constraint effects on *LE*, biases and discrepancies in regional *LE* estimates among *LE_SM*, *LE_RH*, and *LE_DT* could be attributed to the following reasons. First, *ESA CCI SM* biases may influence hybrid *LE* model accuracy, which would lead to estimated *LE* discrepancies among *LE_SM*, *LE_RH*, and *LE_DT*. For example, we found *ESA CCI SM* underestimated *SM* compared to ground measurements at Arou site (Fig. S8) (Wang et al., 2018). Thus, *ESA CCI SM* product biases could have introduced substantial uncertainties into *LE* estimates. Second, although all gridded products were interpolated to 1 km at the regional scale, error propagation through averaging and interpolation could have affected biases and discrepancies in different *LE* estimates. For example, three downscaling methods (bilinear interpolation, Kriging interpolation, and Bayesian maximum entropy) for interpolating *ESA CCI SM* data with 0.25° spatial resolution to 1 km resolution generate 12%, 13%, and 15% *LE* estimation error, respectively. Finally, the regional R_n algorithm derived from gridded data could also introduced *LE* estimation errors and discrepancies in regional *LE* estimates among *LE_SM*, *LE_RH*, and *LE_DT*. The algorithm considers *NDVI* and *RH* influences, which are also included in the satellite derived hybrid *LE* models. Thus, *RH* effects on *LE* are greater than both *DT* and *SM*. Further work is required to compare and explain differences between hybrid model estimate *LE* and other *LE* products.

5. Conclusion

The goal of this study was to develop a suitable satellite-derived hybrid *LE* model to estimate terrestrial *LE* in the Heihe River Basin of Northwest China, and to assess model performance and sensitivity parameterized by three soil moisture constraints: *SM*, *RH* and *DT*. The hybrid *LE* model was trained using observed *LE* over 2012/2013–2014, and validated using observed *LE* for 2015 and leave-one-out cross-validation. We also estimated regional *LE* in *HRB* using the resulting *LE_SM*, *LE_RH*, and *LE_DT* models.

Validation results showed *LE* model differences across the 12 selected flux tower sites, incorporating different land cover types. From the three *SM* constraint schemes investigated, *LE_SM* achieved the highest accuracy in terms of spatial variation compared with *LE_RH*, and *LE_DT*. A satellite-derived hybrid *LE* model using three *SM* constraints may be the most feasible approach to estimate terrestrial LE for different biomes, since *SM*, *RH*, and *DT* could potentially determine LE/R_n variations for various land cover types. Regional *LE* estimation showed large spatial variability for *LE* estimates along with strong seasonal and annual variations, reflecting climate conditions and vegetation distributions controlling effects. The large discrepancies may be attributed to differences in water constraint parameterization within the models. To refine a satellite-derived hybrid model by coupling empirical models and process-based models for improving regional terrestrial *LE*, further work is required to compare and explain differences between hybrid model derived-*LE* and other *LE* products.

Declaration of competing interest

The authors declare they have no conflicts of interest.

Acknowledgements

We thank Dr. Xianhong Xie from Faculty of Geographical Science, Beijing Normal University, China for their suggestions to improve this manuscript. We also thank International Science Editing (http://www.internationalscienceediting.com) for editing this manuscript. We gratefully acknowledge Kun Yang Institute of Tibetan Plateau Research, Chinese Academy of Sciences, and Bo Jiang from Beijing Normal University for providing gridded meteorological and satellite data. The forcing dataset used in this study was developed by Data Assimilation and Modeling Center for Tibetan Multi-spheres, Institute of Tibetan Plateau Research, Chinese Academy of Sciences and this data set is provided by Environmental & Ecological Science Data Center for West China, National Natural Science Foundation of China". Eddy covariance ground-measurements of surface heat fluxes and corresponding meteorological data across *HRB* were provided by *WATER* and *HiWATER* experiments (http://www.heihedata.org/data). We would like to address our appreciation for the *PIs* and staff that are working on these sites. This work was partially supported by the Strategic Priority Research Program of the Chinese Academy of Sciences (No. XDA20100101), the Natural Science Fund of China (No. 41671331) and the National Key Research and Development Program of China (No. 2016YFA0600102 and No. 2017YFC0406002). JBF contributed to this paper from the Jet Propulsion Laboratory, California Institute of Technology, under a contract with the National Aeronautics and Space Administration. California Institute of Technology. Government sponsorship acknowledged. JBF was supported in part by the NASA SUSMAP program.

Appendix A. Supplementary data

Supplementary data to this article can be found online at https://doi.org/10.1016/j.scitotenv.2019.133787.

References

Anderson, M.C., Norman, J.M., Kustas, W.P., Houborg, R., Starks, P.J., Agam, N., 2008. A thermal-based remote sensing technique for routine mapping of land-surface carbon, water and energy fluxes from field to regional scales. Remote Sens. Environ. 112, 4227–4241.

Badgley, G., Fisher, J.B., Jiménez, C., Tu, K.P., Vinukollu, R., 2015. On uncertainty in global terrestrial evapotranspiration estimates from choice of input forcing datasets. J. Hydrometeorol. 16, 1449–1455.

Baldocchi, D., Valentini, R., Running, S.R., Oechel, W., Dahlman, R., 1996. Strategies for measuring and modelling CO_2 and water vapor fluxes over terrestrial ecosystems. Glob. Chang. Biol. 2, 159–168.

Baldocchi, D., Falge, E., Gu, L., Olson, R., Hollinger, D., Running, S., et al., 2001. FLUXNET: a new tool to study the temporal and spatial variability of ecosystem-scale carbon dioxide, water vapor and energy flux densities. Bull. Am. Meteorol. Soc. 82, 2415–2434.

Bouchet, R., 1963. Evapotranspiration re'elle evapotranspiration potentielle, signification climatique. Int. Assoc. Sci. Hydrol. 134–142.

Brutsaert, W., 2005. Hydrology: An Introduction. Cambridge University Press, Cambridge, p. 605.

Chen, F., Dudhia, J., 2001. Coupling an advanced land surface -hydrology model with the Penn State-NCAR MM5 modeling system. Part I: model implementation and sensitivity. Mon. Weather Rev. 129, 569–585.

Cheng, G., Xiao, H., Chen, Y., 2010. Research on the Ecology-Hydrology of Typical Inland River in the West of China. China Meteorological Press, Beijing.

Cheng, G., Li, X., Zhao, W., Xu, Z., Feng, Q., Xiao, S., Xiao, H., 2014. Integrated study of the water-ecosystem-economy in the Heihe river basin. Natl. Sci. Rev. 1, 413–428.

Cleugh, H.A., Leuning, R., Mu, Q., Running, S.W., 2007. Regional evaporation estimates from flux tower and MODIS satellite data. Remote Sens. Environ. 106, 285–304.

Dorigo, W., Wagner, W., Albergel, C., Albrecht, F., Balsamo, G., Brocca, L., et al., 2017. ESA CCI soil moisture for improved earth system understanding: state-of-the art and future directions. Remote Sens. Environ. 203, 185–215.

Ershadi, A., McCabe, M., Evans, J., Chaney, N., Wood, E., 2014. Multi-site evaluation of terrestrial evaporation models using FLUXNET data. Agric. For. Meteorol. 187, 46–61.

Fisher, J.B., Tu, K.P., Baldocchi, D.D., 2008. Global estimates of the land atmosphere water flux based on monthly AVHRR and ISLSCP-II data, validated at 16 FLUXNET sites. Remote Sens. Environ. 112, 901–919.

Fisher, J.B., Melton, F., Middleton, E., Hain, C., Anderson, M., Allen, R., et al., 2017. The future of evapotranspiration: global requirements for ecosystem functioning, carbon and climate feedbacks, agricultural management, and water resources. Water Resour. Res. 53, 2618–2626.

Foken, T., 2008. The energy balance closure problem: an overview. Ecol. Appl. 18, 1351–1367.

Gao, X., Dirmeyer, P., 2006. A multimodel analysis, validation, and transferability study of global soil wetness products. J. Hydrometeorol. 7, 1218–1236.

García, M., Sandholt, I., Ceccato, P., Ridler, M., Mougin, E., Kergoat, L., et al., 2013. Actual evapotranspiration in drylands derived from in-situ and satellite data: assessing biophysical constraints. Remote Sens. Environ. 131, 103–118.

Glenn, E.P., Morino, K., Didan, K., Jordan, F., Carroll, K.C., Nagler, P.L., Hultine, K., Sheader, L., Waugh, J., 2008. Scaling sap flux measurements of grazed and ungrazed shrub communities with fine and coarse-resolution remote sensing. Ecohydrology 1, 316–329.

Hu, G., Jia, L., Menenti, M., 2015a. Comparison of MOD16 and LSA-SAF MSG evapotranspiration products over Europe for 2011. Remote Sens. Environ. 156, 510–526.

Hu, X.L., Lu, L., Li, X., Wang, J.H., Lu, X.G., 2015b. Ejin oasis land use and vegetation change between 2000 and 2011: the role of the ecological water diversion project. Energies 8, 7040–7057.

Huete, A., Didan, K., Miura, T., Rodriguez, E.P., Gao, X., Ferreira, L.G., 2002. Overview of the radiometric and biophysical performance of the MODIS vegetation indices. Remote Sens. Environ. 83, 195–213.

Hui, D., Wan, S., Su, B., Katul, G., Monson, R., Luo, Y., 2004. Gap-filling missing data in eddy covariance measurements using multiple imputation (MI) for annual estimations. Agric. For. Meteorol. 121, 93–111.

Idso, S.B., Brazel, A.J., 1984. Rising atmospheric carbon dioxide concentrations may increase stream flow. Nature 312, 51–53.

Jackson, R., Reginato, R., Idso, S., 1977. Wheat canopy temperature: a practical tool for evaluating water requirements. Water Resour. Res. 13, 651–656.

Jiménez, C., Prigent, C., Mueller, B., Seneviratne, S.I., McCabe, M.F., Wood, E.F., et al., 2011. Global intercomparison of 12 land surface heat flux estimates. J. Geophys. Res. Atmos. 116, D02102.

Jin, Y., Randerson, J., Goulden, M., 2011. Continental-scale net radiation and evapotranspiration estimated using MODIS satellite observations. Remote Sens. Environ. 115, 2302–2319.

Jung, M., Reichstein, M., Ciais, P., Seneviratne, S., Sheffield, J., Goulden, M., et al., 2010. Recent decline in the global land evapotranspiration trend due to limited moisture supply. Nature 467, 951–954.

Jung, M., Reichstein, M., Margolis, H., Cescatti, A., Richardson, A., Altaf Arain, M., et al., 2011. Global patterns of land-atmosphere fluxes of carbon dioxide, latent heat, and sensible heat derived from eddy covariance, satellite, and meteorological observations. J. Geophys. Res. Atmos. 116, G00J07.

Kalma, J., McVicar, T.R., McCabe, M., 2008. Estimating land surface evaporation: a review of methods using remotely sensed surface temperature data. Surv. Geophys. 29, 421–469.

Li, X., Li, X.W., Li, Z., Ma, M., Wang, J., Xiao, Q., et al., 2009a. Watershed allied telemetry experimental research. J. Geophys. Res. Atmos. 114, D22103.

Li, Z., Tang, R., Wan, Z., Bi, Y., Zhou, C., Tang, B., Yan, G., Zhang, X., 2009b. A review of current methodologies for regional evapotranspiration estimation from remotely sensed data. Sensors 9, 3801–3853.

Li, X., Cheng, G., Liu, S., Xiao, Q., Ma, M., Jin, R., et al., 2013. Heihe watershed allied telemetry experimental research (HiWATER): scientific objectives and experimental design. Bull. Am. Meteorol. Soc. 94, 1145–1160.

Li, X., Cheng, G., Ge, Y., Li, H., Han, F., Hu, X., et al., 2018. Hydrological cycle in the Heihe River basin and its implication for water resource management in endorheic basins. J. Geophys. Res. Atmos. 123, 890–914.

Liu, S., Xu, Z., Wang, W., Jia, Z., Zhu, M., Bai, J., Wang, J., 2011. A comparison of eddy covariance and large aperture scintillometer measurements with respect to the energy balance closure problem. Hydrol. Earth Syst. Sci. 15, 1291–1306.

Liu, S., Xu, Z., Zhu, Z., Jia, Z., Zhu, M., 2013. Measurements of evapotranspiration from eddy-covariance systems and large aperture scintillometers in the Hai River basin, China. J. Hydrol. 487, 24–38.

Liu, S., Li, X., Xu, Z., Che, T., Xiao, Q., Ma, M., et al., 2018a. The Heihe integrated observatory network: a basin-scale land surface processes observatory in China. Vadose Zone J. 17, 180072. https://doi.org/10.2136/vzj2018.04.0072.

Liu, Y., Xiao, J., Ju, W., Zhu, G., Wu, X., Fan, W., Li, D., Zhou, Y., 2018b. Satellite-derived LAI products exhibit large discrepancies and can lead to substantial uncertainty in simulated carbon and water fluxes. Remote Sens. Environ. 206, 174–188.

McVicar, T.R., Jupp, D.L.B., 2002. Using covariates to spatially interpolate moisture availability in the Murray-Darling basin: a novel use of remotely sensed data. Remote Sens. Environ. 79, 199–212.

McVicar, T., Roderick, M., Donohue, R., Li, L., Van Niel, T., Thomas, A., et al., 2012. Global review and synthesis of trends in observed terrestrial near-surface wind speeds: implications for evaporation. J. Hydrol. 416-417, 182–205.

Miralles, D., Holmes, T., De Jeu, R., Gash, J., Meesters, A., Dolman, A., 2011. Global land surface evaporation estimated from satellite-based observations. Hydrol. Earth Syst. Sci. 15, 453–469.

Mu, Q., Heinsch, F., Zhao, M., Running, S., 2007. Development of a global evapotranspiration algorithm based on MODIS and global meteorology data. Remote Sens. Environ. 111, 519–536.

Mu, Q., Zhao, M., Running, S., 2011. Improvements to a MODIS global terrestrial evapotranspiration algorithm. Remote Sens. Environ. 115, 1781–1800.

Mueller, B., Seneviratne, S.I., Jiménez, C., Corti, T., Hirschi, M., Balsamo, G., et al., 2011. Evaluation of global observations-based evapotranspiration datasets and IPCC AR4 simulations. Geophys. Res. Lett. 38, L06402.

Nagler, P., Cleverly, J., Lampkin, D., Glenn, E., Huete, A., Wan, Z., 2005. Predicting riparian evapotranspiration from MODIS vegetation indices and meteorological data. Remote Sens. Environ. 94, 17–30.

Norman, J., Kustas, W., Humes, K., 1995. Source approach for estimating soil and vegetation energy fluxes in observations of directional radiometric surface temperature. Agric. For. Meteorol. 77, 263–293.

Overgaard, J., Rosbjerg, D., Butts, M.B., 2006. Land-surface modelling in hydrological perspective—a review. Biogeosciences 3, 229–241.

Pan, X.D., Li, X., Shi, X.K., Han, X.J., Luo, L.H., Wang, X., 2012. Dynamic downscaling of near-surface air temperature at the basin scale using WRF-a case study in the Heihe River basin, China. Front. Earth Sci. 6, 314–323.

Pipunic, R., Walker, J., Western, A., 2008. Assimilation of remotely sensed data for improved latent and sensible heat flux prediction: a comparative synthetic study. Remote Sens. Environ. 112, 1295–1305.

Polhamus, A.M., Fisher, J.B., Tu, K.P., 2012. What controls the error structure in evapotranspiration models? Agric. For. Meteorol. 169, 12–24.

Priestley, C., Taylor, R., 1972. On the assessment of surface heat flux and evaporation using large-scale parameters. Mon. Weather Rev. 100, 81–92.

Purdy, A.J., Fisher, J.B., Goulden, M.L., Colliander, A., Halverson, G., Tu, K., Famiglietti, J.S., 2018. SMAP soil moisture improves global evapotranspiration. Remote Sens. Environ. 219, 1–14.

Robock, A., Luo, L., Wood, E.F., Wen, F., Mitchell, K.E., Houser, P.R., et al., 2003. Evaluation of the North American land data assimilation system over the southern Great Plains during the warm season. J. Geophys. Res. Atmos. 108 (D22), 8846.

Seneviratne, S.I., Corti, T., Davin, E.L., Hirschi, M., Jaeger, E.B., Lehner, I., Orlowsky, B., Teuling, A.J., 2010. Investigating soil moisture-climate interactions in a changing climate: a review. Earth-Sci. Rev. 99, 125–161.

Shuttleworth, W.J., 2007. Putting the “vap” into evaporation. Hydrol. Earth Syst. Sci. 11, 210–244.

Si, J.H., Feng, Q., Zhang, X.Y., Chang, Z.Q., Su, Y.H., Xi, H.Y., 2007. Sap flow of Populus euphratica in a desert riparian forest in an extreme arid region during the growing season. J. Integrative Plant Biol. 49, 425–436.

Skamarock, W., Klemp, J., 2008. A time-split nonhydrostatic atmospheric model for weather research and forecasting applications. J. Comput. Phys. 227, 3465–3485.

Song, L., Liu, S., Kustas, W.P., Nieto, H., Sun, L., Xu, Z., Skaggs, T.H., Ma, M., Xu, T., Tang, X., Li, Q., 2018. Monitoring and validating spatially and temporally continuous daily evaporation and transpiration at river basin scale. Remote Sens. Environ. 219, 72–88.

Twine, T.E., Kustas, W.P., Norman, J.M., Cook, D.R., Houser, P.R., Meyers, T.P., Prueger, J.H., Starks, P.J., Wesely, M.L., 2000. Correcting eddy covariance flux underestimates over a grassland. Agric. For. Meteorol. 103, 279–300.

Vinukollu, R.K., Wood, E.F., Ferguson, C.R., Fisher, J.B., 2011. Global estimates of evapotranspiration for climate studies using multi-sensor remote sensing data: evaluation of three process-based approaches. Remote Sens. Environ. 115, 801–823.

Wang, K., Dickinson, R., 2012. A review of global terrestrial evapotranspiration: observation, modeling, climatology, and climatic variability. Rev. Geophys. 50 (RG2005).

Wang, K., Liang, S., 2008. An improved method for estimating global evapotranspiration based on satellite determination of surface net radiation, vegetation index, temperature, and soil moisture. J. Hydrometeorol. 9, 712–727.

Wang, K., Liang, S., 2009. Estimation of daytime net radiation from shortwave radiation measurements and meteorological observations. J. Appl. Meteorol. Clim. 48, 634–643.

Wang, K., Wang, P., Li, Z., Sparrow, M., Cribb, M., 2007. A simple method to estimate evapotranspiration from a combination of net radiation, vegetation indices and temperatures. J. Geophys. Res. Atmos. 112, D15107.

Wang, K., Dickinson, R., Wild, M., Liang, S., 2010. Evidence for decadal variation in global terrestrial evapotranspiration between 1982 and 2002: 1. Model development. J. Geophys. Res. Atmos. 115, D20112.

Wang, Y., An, R., You, J., Wang, Z., 2018. Downscaling and merging of the CCI soil moisture product over. China. J. Hohai Univ. (Nat. Sci). 46, 186–202.

Xiao, J., Zhuang, Q., Baldocchi, D.D., Law, B.E., Richardson, A.D., Chen, J., et al., 2008. Estimation of net ecosystem carbon exchange for the conterminous United States by combining MODIS and AmeriFlux data. Agric. For. Meteorol. 148, 1827–1847.

Xiao, J., Zhuang, Q., Law, B.E., Chen, J., Baldocchi, D., Cook, D.R., et al., 2010. A continuous measure of gross primary production for the conterminous United States derived from MODIS and AmeriFlux data. Remote Sens. Environ. 114, 576–591.

Xie, X., Liang, S., Yao, Y., Jia, K., Meng, S., Li, J., 2015. Detection and attribution of changes in hydrological cycle over the Three-North region of China: climate change versus afforestation effect. Agric. For. Meteorol. 203, 74–87.

Xiong, Y., Zhao, S., Tian, F., Qiu, G., 2015. An evapotranspiration product for arid regions based on the three-temperature model and thermal remote sensing. J. Hydrol. 530, 392–404.

Xu, T., Liang, S., Liu, S., 2011a. Estimating turbulent fluxes through assimilation of geostationary operational environmental satellites data using ensemble Kalman filter. J. Geophys. Res. Atmos. 116, D09109.

Xu, T., Liu, S., Liang, S., Qin, J., 2011b. Improving predictions of water and heat fluxes by assimilating MODIS land surface temperature products into common land model. J. Hydrometeorol. 12, 227–244.

Xu, Z., Liu, S., Li, X., Shi, S., Wang, J., Zhu, Z., Xu, T., Wang, W., Ma, M., 2013. Intercomparison of surface energy flux measurement systems used during the HiWATER-MUSOEXE. J. Geophys. Res. Atmos. 118, 13140–13157.

Yan, H., Shugart, H.H., 2010. An air relative-humidity-based evapotranspiration model from eddy covariance data. J. Geophys. Res. Atmos. 115, D16106.

Yang, F., White, M., Michaelis, A., Ichii, K., Hashimoto, H., Votava, P., Zhu, A.X., Nemani, R.R., 2006. Prediction of continental-scale evapotranspiration by combining MODIS and AmeriFlux data through support vector machine. IEEE Trans. Geosci. Remote Sens. 44, 3452–3461.

Yao, Y., Liang, S., Cheng, J., Liu, S., Fisher, J.B., Zhang, X., et al., 2013. MODIS-driven estimation of terrestrial latent heat flux in China based on a modified Priestley-Taylor algorithm. Agric. For. Meteorol. 171-172, 187–202.

Yao, Y., Liang, S., Li, X., Hong, Y., Fisher, J.B., Zhang, N., et al., 2014. Bayesian multimodel estimation of global terrestrial latent heat flux from eddy covariance, meteorological, and satellite observations. J. Geophys. Res. Atmos. 119, 4521–4545.

Yao, Y., Liang, S., Li, X., Chen, J., Wang, K., Jia, K., et al., 2015. A satellite-based hybrid algorithm to determine the Priestley-Taylor parameter for global terrestrial latent heat flux estimation across multiple biomes. Remote Sens. Environ. 165, 216–233.

Yao, Y., Liang, S., Li, X., Chen, J., Liu, S., Jia, K., et al., 2017a. Improving global terrestrial evapotranspiration estimation using support vector machine by integrating three process-based algorithms. Agric. For. Meteorol. 242, 55–74.

Yao, Y., Liang, S., Yu, J., Chen, J., Liu, S., Lin, Y., et al., 2017b. A simple temperature domain two-source model for estimating agricultural field surface energy fluxes from Landsat images. J. Geophys. Res. Atmos. 122, 5211–5236.

Yao, Y., Liang, S., Cao, B., Liu, S., Yu, G., Jia, K., Zhang, X., et al., 2018. Satellite detection of water stress effects on terrestrial latent heat flux with MODIS shortwave infrared reflectance data. J. Geophys. Res. Atmos. 123, 11410–11430.

Yebra, M., Dijk, A., Leuning, R., Huete, A., Guerschman, J., 2013. Evaluation of optical remote sensing to estimate actual evapotranspiration and canopy conductance. Remote Sens. Environ. 129, 250–261.

Yuan, W., Liu, S., Yu, G., Bonnefond, J.-M., Chen, J., Davis, K., et al., 2010. Global estimates of evapotranspiration and gross primary production based on MODIS and global meteorology data. Remote Sens. Environ. 114, 1416–1431.

Zhang, R., Sun, X., Zhu, Z., Su, H., Tang, X., 2003. A remote sensing model for monitoring soil evaporation based on thermal inertia and its validation. Sci. China Ser. D. 46, 342–355.

Zhang, K., Kimball, J., Nemani, R., Running, S., 2010. A continuous satellite-derived global record of land surface evapotranspiration from 1983 to 2006. Water Resour. Res. 46, W09522.

Zhong, B., Ma, P., Nie, A., Yang, A., Yao, Y., Lv, W., Zhang, H., Liu, Q., 2014. Land cover mapping using time series HJ-1/CCD data. Sci. China Earth Sci. 57, 1790–1799.

Zhou, Y., Li, X., Yang, K., Zhou, J., 2018. Assessing the impacts of an ecological water diversion project on water consumption through high-resolution estimations of actual evapotranspiration in the downstream regions of the Heihe River basin. China. Agric. For. Meteorol. 249, 210–227.